ACS APPLIED MATERIALS & INTERFACES

www.acsami.org

Research Article

Substrate-Free Thermoelectric 25 μm-Thick Ag_2Se Films with High Flexibility and In-Plane zT of 0.5 at Room Temperature

Dongchan Lee,[‖] Woomin Park,[‖] Yeong A Kang, Hyeong Taek Lim, Seungbeom Park, Yeongjun Mun, Jungwon Kim,* and Kwang-Suk Jang*

Cite This: *ACS Appl. Mater. Interfaces* 2023, 15, 3047−3053

Read Online

ACCESS | Metrics & More | Article Recommendations | Supporting Information

ABSTRACT: Thermoelectric inorganic films are flexible when sufficiently thin. By removing the substrate, that is, making them free-standing, the flexibility of thermoelectric films can be enhanced to the utmost extent. However, studies on the flexibility of free-standing thermoelectric inorganic films have not yet been reported. Herein, the high thermoelectric performance and flexibility of free-standing thermoelectric Ag_2Se films are reported. Free-standing Ag_2Se films with a thickness of 25.0 ± 3.9 μm exhibited an in-plane zT of 0.514 ± 0.060 at room temperature. These films exhibited superior flexibility compared to Ag_2Se films constrained on a substrate. The flexibility of the Ag_2Se films was systematically investigated in terms of bending strain, bending radius, thickness, and elastic modulus. Using free-standing Ag_2Se films, a substrate-free, flexible thermoelectric generator was fabricated. The energy-harvesting capacity of the thermoelectric generator was also demonstrated.

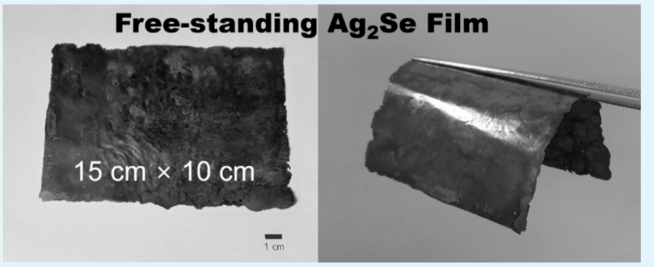

KEYWORDS: *flexible thermoelectrics, silver selenide, Ag_2Se, free-standing films, in-plane thermal conductivity*

INTRODUCTION

Thermoelectric materials have been extensively studied for application in devices that convert thermal energy into electrical energy and vice versa. Thermoelectric materials should possess a high Seebeck coefficient ($S = -\Delta V/\Delta T$), high electrical conductivity (σ), and low thermal conductivity (κ). The performance of the thermoelectric materials at a given temperature (T) is evaluated using the dimensionless figure of merit ($zT = S^2\sigma T/\kappa$). Although the power factor (PF = $S^2\sigma$) has been proposed as an alternative for evaluating the performance of thermoelectric materials, its use is undesirable due to inaccurate results. Traditional thermoelectric materials that exhibit high performance at near-room temperature, such as Bi_2Te_3, are inorganic and brittle. Therefore, the development of flexible thermoelectric materials that exhibit high performance at near-room temperature has attracted attention because they can be applied to flexible thermoelectric devices such as wearable thermoelectric generators and Peltier coolers.[1−17]

The bending strain of free-standing films is inversely proportional to the film thickness; therefore, brittle materials exhibit flexibility when they are sufficiently thin.[1] Recently, inorganic thermoelectric films have attracted significant attention as flexible thermoelectric materials.[4−12] For example, Saeidi-Javash et al. reported that 0.65 μm thick $Bi_2Te_{2.7}Se_{0.3}$ films deposited on polyimide films using $Bi_2Te_{2.7}Se_{0.3}$ nanoplates exhibited excellent flexibility and a room-temperature PF of 730 μW m^{-1} K^{-2}.[6] Recently, Ag_2Se films have emerged as promising flexible thermoelectric materials with high n-type PF.[9−12] For example, Ding et al. reported that 10 μm thick Ag_2Se films deposited on nylon membrane filters using Ag_2Se nanowires exhibited excellent flexibility and a room-temperature PF of 987.4 μW m^{-1} K^{-2}.[9] Because thermoelectric inorganic films, such as Ag_2Se films, are brittle, their thickness is a critical parameter for determining their flexibility. If thermoelectric films are constrained on a substrate, their flexibility should be affected by the type and thickness of the substrate, as well as the thermoelectric film thickness. For example, in the bent state, an additional bending strain that originates from the substrate thickness should be applied to a thermoelectric film constrained on a substrate. Thus, the absence of a substrate is desirable for maximizing flexibility. Although the presence or absence of a substrate plays a crucial role in determining the flexibility, such research has not yet been reported. In addition, from a practical viewpoint, the use of flexible thermoelectric films without a substrate, that is, free-standing films, is desirable for zT evaluation and device applications. PF has been used as an alternative to zT because it is difficult to measure the in-plane thermal conductivity of a

Received: November 8, 2022
Accepted: December 22, 2022
Published: January 4, 2023

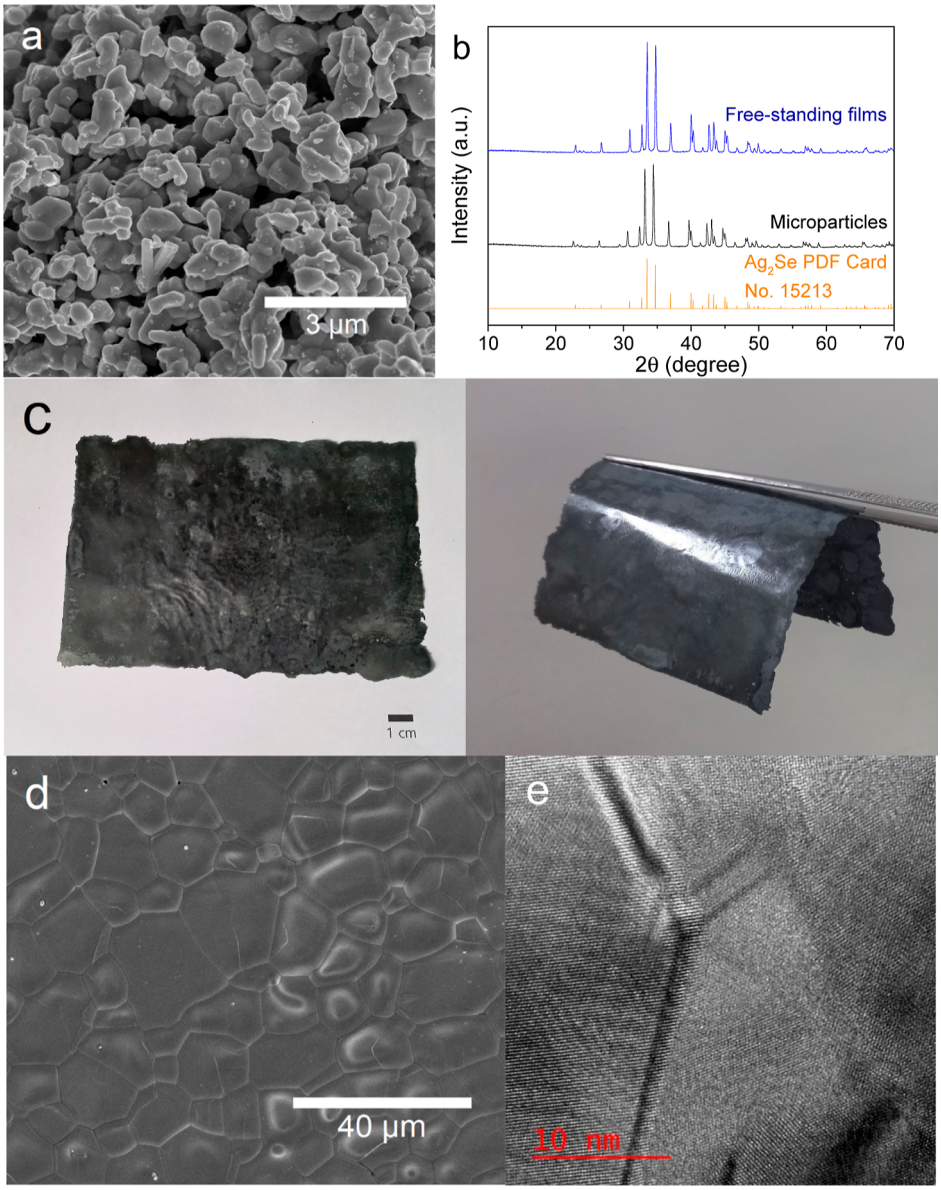

Figure 1. (a) SEM image of Ag_2Se microparticles. (b) XRD patterns of Ag microparticles and free-standing Ag_2Se film. (c) Photos of flexible, free-standing Ag_2Se films. (d) SEM and (e) cross-section TEM images of the free-standing Ag_2Se film.

film constrained on a substrate.[6−11] The substrate volume can restrict the electrical connection and high-density integration of thermoelectric materials, which significantly affects the performance of thermoelectric devices.[18−21]

In this study, we report the high thermoelectric performance and flexibility of substrate-free free-standing Ag_2Se films. Free-standing Ag_2Se films were fabricated by drop-casting a well-dispersed Ag_2Se microparticle ink on a polyimide substrate, followed by hot pressing and peeling off from the substrate. The absence of a substrate facilitates the direct measurement of the in-plane thermoelectric performance and enhances the flexibility of the Ag_2Se films. The free-standing Ag_2Se films with a thickness of 25.0 ± 3.9 μm exhibited an in-plane thermal conductivity and zT of 0.892 ± 0.071 W m^{-1} K^{-1} and 0.514 ± 0.060, respectively, at room temperature. The free-standing Ag_2Se films exhibited superior flexibility compared to Ag_2Se films constrained on a substrate. The flexibility of the Ag_2Se films was systematically investigated in terms of bending strain, bending radius, thickness, and elastic modulus. Using free-standing Ag_2Se films, a substrate-free, flexible thermoelectric generator was fabricated. The energy-harvesting capacity of the thermoelectric generator was demonstrated.

RESULTS AND DISCUSSION

Ag_2Se microparticles were obtained via gram-scale synthesis. Figure 1a shows the scanning electron microscopy (SEM) image of Ag_2Se microparticles with irregular shapes and dimensions of less than 1 μm. The X-ray diffraction (XRD) peaks of Ag_2Se microparticles match well with those of crystalline Ag_2Se (Figure 1b). The average crystal grain size of Ag_2Se microparticles was calculated to be 48 nm from the (112) XRD peak using the Scherrer equation. The Ag/Se ratio of the Ag_2Se microparticles was measured to be 2.0/1.0 using inductively coupled plasma optical emission spectroscopy (ICP−OES). A well-dispersed Ag_2Se microparticle/chloroform ink was prepared using the ball mill process. Ag_2Se microparticles were uniformly deposited on a polyimide substrate via drop casting. Flexible, free-standing Ag_2Se films

https://doi.org/10.1021/acsami.2c20115
ACS Appl. Mater. Interfaces 2023, 15, 3047−3053

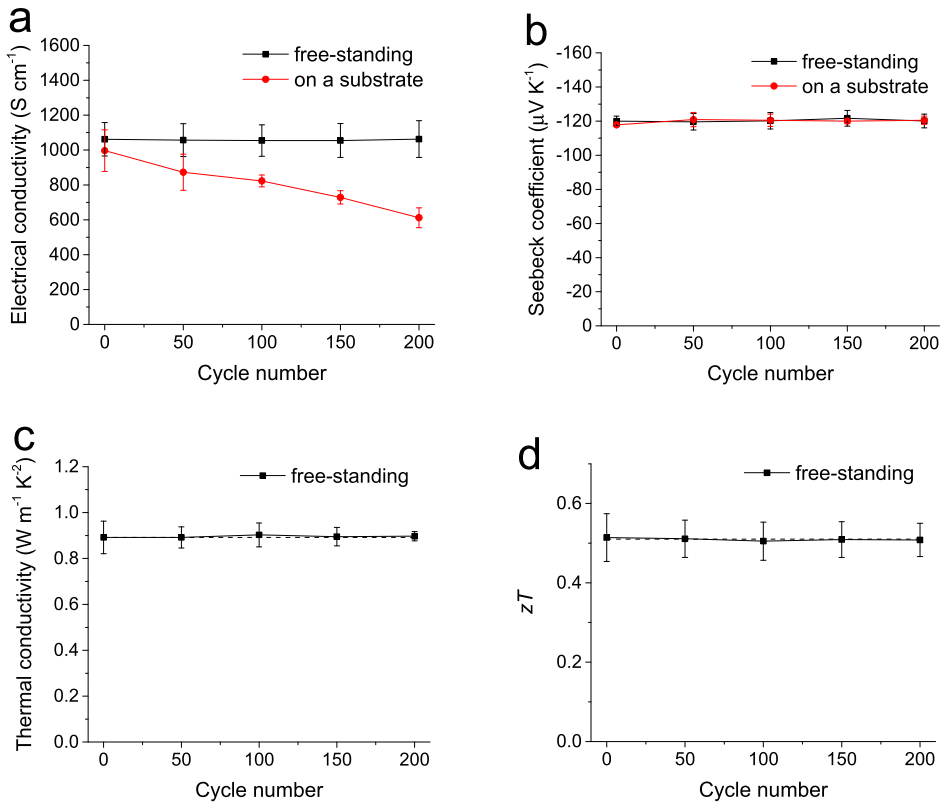

Figure 2. Bending cycle number-dependent (a) electrical conductivity, (b) Seebeck coefficient, (c) thermal conductivity, and (d) zT of free-standing Ag_2Se films and Ag_2Se films constrained on a substrate.

were fabricated, followed by hot pressing at 230 °C and 5 MPa, and then peeling off from the substrate (Figure 1c). To demonstrate size scalability and potential mass production, a free-standing Ag_2Se film with a size of 15 cm × 10 cm was prepared. Thermoelectric Ag_2Se films were also prepared using a previously reported vacuum filtration method.[9,10] However, only Ag_2Se films constrained on a membrane filter substrate with a small area can be obtained. Figure 1d shows the SEM image of the freestanding Ag_2Se film, where the Ag_2Se microparticles are pressed flat and condensed with each other. The diameters of the pressed particulates are in the range of 0.3 to 2 μm. The broad size distribution originates from the broad size distribution of Ag_2Se microparticles. There is a negligible difference between the XRD patterns of the Ag_2Se microparticles and free-standing films (Figure 1b). The average crystal grain size of 48 nm was left unchanged using the drop-casting and hot-pressing processes. Figure 1e shows the cross-sectional transmission electron microscopy (TEM) image of the Ag_2Se film. The nanocrystalline domains and grain boundaries are clearly visible. To show the chemical bonding states of the free-standing Ag_2Se film, X-ray photoelectron spectroscopy (XPS) analysis was performed (Figure S1). In the Ag 3d XPS spectrum, there are two isolated peaks at 373.6 and 367.6 eV, which correspond to the intense spin−orbit doublet of Ag $3d_{3/2}$ and Ag $3d_{5/2}$ with a spin−orbit splitting of 6.0 eV.[22,23] The Se 3d XPS spectrum consists of two peaks at 55.5 and 54.6 eV, which correspond to the spin−orbit doublet of Se $3d_{3/2}$ and Se $3d_{5/2}$ with a spin−orbit splitting of 0.9 eV.[23,24] The peak attributed to Se 3d from SeO_2 occurs at ∼59.9 eV.[25] However, there is no further peak in the Se 3d XPS spectrum, which indicates the absence of selenium oxide on the surface of the free-standing Ag_2Se film.

The in-plane thermoelectric performance of the free-standing Ag_2Se films at room temperature was investigated (Figure 2). Free-standing Ag_2Se films with a thickness of 25.0 ± 3.9 μm exhibit an n-type Seebeck coefficient of 120 ± 3 μV K^{-1}. To verify the accuracy of the Seebeck coefficient measured using our custom-built measurement system, the Seebeck coefficient of the free-standing Ag_2Se film was also measured using commercial equipment. The n-type Seebeck coefficient measured using Linseis LSR-3 equipment (121 μV K^{-1}) is coterminous with that measured using a custom-built measurement system. The in-plane electrical conductivity, carrier concentration, and mobility of the free-standing Ag_2Se films were 1060 ± 100 S cm^{-1}, −4.79 ± 0.41 × 10^{18} cm^{-3}, and 1390 ± 90 cm^2 V^{-1} s^{-1}, respectively. The Seebeck coefficient and electrical conductivity at room temperature were comparable to those of bulk Ag_2Se.[26−30] The free-standing Ag_2Se films exhibited an in-plane thermal conductivity of 0.892 ± 0.071 W m^{-1} K^{-1} at room temperature. Thermal conductivity is the sum of the electronic and lattice (phonon) contributions. Using the Wiedemann−Franz-Lorenz relationship, the average electronic thermal conductivity of the free-standing Ag_2Se films was calculated to be 0.758 W m^{-1} K^{-1}. Thus, the free-standing Ag_2Se films exhibited a thermal conductivity of 0.134 W m^{-1} K^{-1}, which is lower than those of bulk Ag_2Se, 0.22−0.70 W m^{-1} K^{-1}.[26−30] The lower lattice thermal conductivity might be attributed to phonon scattering at the grain boundaries of small crystals and interfaces of the pressed particulates. The free-standing Ag_2Se films exhibited an excellent in-plane zT of 0.514 ± 0.060 at room temperature. For comparison, Ag_2Se films constrained on a membrane filter substrate were also fabricated (Figure S2). These films exhibited an n-type Seebeck coefficient and an electrical

https://doi.org/10.1021/acsami.2c20115
ACS Appl. Mater. Interfaces 2023, 15, 3047−3053

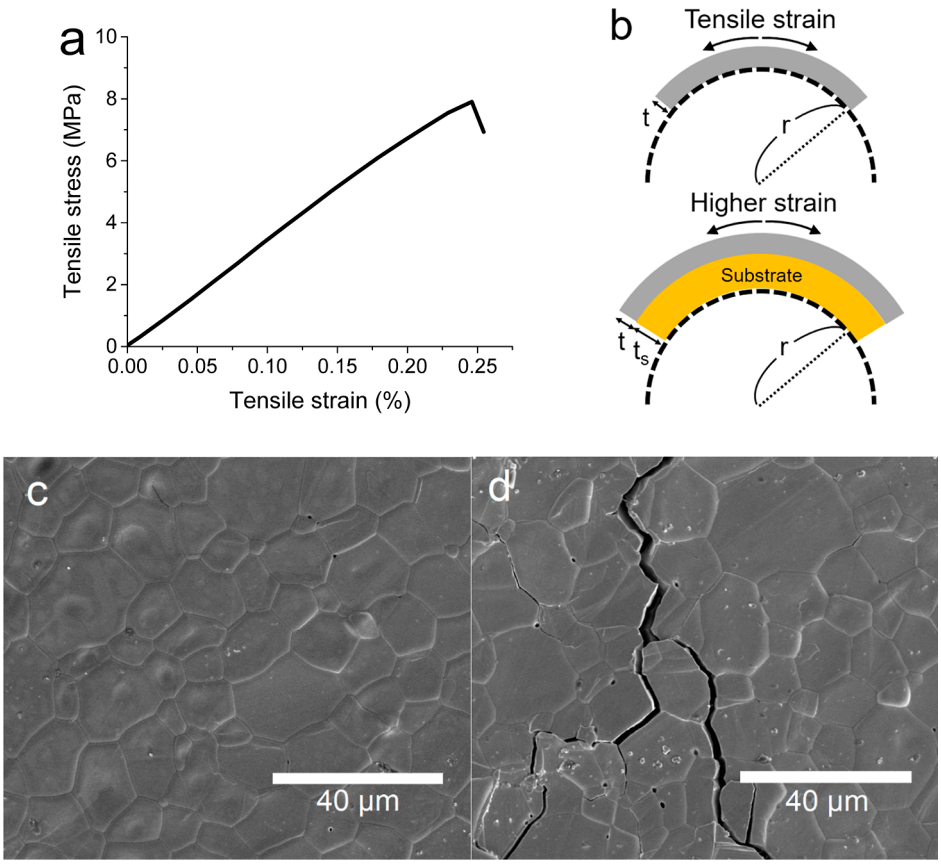

Figure 3. (a) Tensile stress−strain curve of free-standing Ag_2Se film. (b) Schematic of the bent state of free-standing Ag_2Se film and Ag_2Se film constrained on a substrate. SEM images of the (c) free-standing Ag_2Se film and (d) Ag_2Se film constrained on a substrate after 200 bending cycles.

conductivity of 118 ± 1 μV K^{-1} and 997 ± 119 S cm^{-1}, respectively, which are comparable to those of free-standing Ag_2Se films. However, the zT of Ag_2Se films on a substrate could not be obtained because the in-plane thermal conductivity of films constrained on a substrate cannot be measured directly. To investigate the chemical stabilities, the free-standing Ag_2Se films were immersed in water, ethanol, 1 M aqueous HCl, and 1 M aqueous NaOH for 1 h, respectively, and dried overnight in vacuo. The electrical conductivity and Seebeck coefficient of the free-standing Ag_2Se films were maintained fairly well after the chemical treatments (Figure S3). The free-standing Ag_2Se films exhibited good chemical stabilities, which could make them more useful for practical applications.

To investigate the mechanical properties of the free-standing Ag_2Se film, a tensile test was performed. Figure 3a shows the tensile stress−strain curve of the free-standing Ag_2Se film. The free-standing Ag_2Se film exhibits a brittle nature without ductility. In addition, the film exhibits elastic deformation within a tensile strain of 0.25%. The bending strain applied to free-standing films can be expressed as follows

$$\varepsilon_f = \frac{t}{2r} \quad (1)$$

where t and r are the film thickness and the bending radius, respectively. Thus, brittle materials, such as Ag_2Se, are flexible when they are sufficiently thin. When bent, tensile bending strain was applied to the upper surface of the free-standing film (Figure 3b). For the free-standing Ag_2Se film with a thickness of 25.0 μm and an elastic limit strain of 0.25%, the elastic limit bending radius was calculated to be 5.0 mm. At a bending radius smaller than 5.0 mm, plastic deformation occurs, causing a decrease in the thermoelectric performance. For the flexibility test, we used a bending radius of 5 mm, which was the elastic limit. The flexibilities of the free-standing Ag_2Se films and Ag_2Se films constrained on a substrate were evaluated. The effects of repetitive bending with a radius of 5 mm on the thermoelectric performance were analyzed (Figure 2). The electrical conductivity, Seebeck coefficient, thermal conductivity, and zT of the free-standing Ag_2Se films were well maintained over 200 bending cycles. However, Ag_2Se films constrained on a substrate show relatively poor flexibility. By repetitive bending deformation, the electrical conductivity of Ag_2Se films on the substrate decreased gradually. However, the Seebeck coefficient of the Ag_2Se films on a substrate was maintained. Thus, the Seebeck coefficient may be less affected by mechanical damage. For films constrained on a substrate, a higher bending strain was applied at the given bending radius (Figure 3b). The bending strain applied to the films on the substrate is expressed as follows

$$\varepsilon_c = \frac{(t + t_s)}{2r} \frac{(1 + 2\eta + \chi\eta^2)}{(1 + \eta)(1 + \chi\eta)} \quad (2)$$

where t_s, η, and χ are the substrate thickness, film thickness divided by the substrate thickness, and the elastic modulus of the film divided by the elastic modulus of the substrate, respectively.[31,32] The elastic moduli of the free-standing Ag_2Se film and substrate, 3290 and 638 MPa, respectively, were obtained from the tensile stress−strain curves (Figures 3a and S4). Using a bending radius of 5 mm, the applied bending

https://doi.org/10.1021/acsami.2c20115
ACS Appl. Mater. Interfaces 2023, 15, 3047−3053

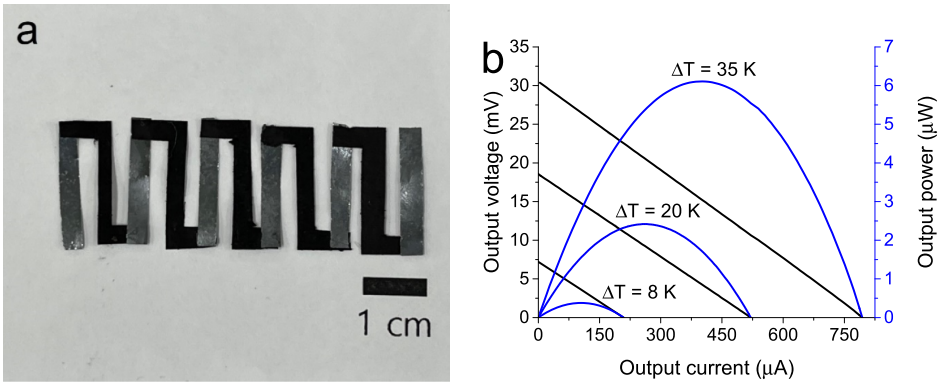

Figure 4. (a) Photo and (b) output voltage−output current and output power−output current curves of substrate-free, flexible thermoelectric generator.

strains of the free-standing Ag_2Se film and Ag_2Se film on a substrate were calculated to be 0.25 and 0.67%, respectively. An additional bending strain that originates from the substrate thickness should be applied to films constrained on a substrate. The bending strain applied to the Ag_2Se film on a substrate was significantly higher than the elastic limit strain. Thus, plastic deformation and mechanical damage occurred after bending. Figure 3c,d shows the SEM images of the free-standing Ag_2Se film and Ag_2Se film on a substrate after 200 bending cycles, respectively. The surface morphology of the free-standing Ag_2Se film was not affected by the bending deformation. However, cracks were observed on the surface of the Ag_2Se film constrained on a substrate. The decrease in electrical conductivity might have originated from the cracks formed by the bending strain being higher than the elastic limit strain. We can conclude that the free-standing Ag_2Se films exhibit superior flexibility compared to Ag_2Se films constrained on a substrate. By making it free-standing, the flexibility of thermoelectric films can be greatly enhanced.

Using the free-standing Ag_2Se film as an n-type thermoelectric element, a substrate-free flexible thermoelectric generator was fabricated (Figure 4a). A free-standing, single-walled carbon nanotube (SWCNT) film was used as the p-type thermoelectric element (Figure S5).[18] The Seebeck coefficient and electrical conductivity of the SWCNT films with a thickness of 18.9 ± 0.9 μm were measured to be 21.9 ± 0.3 $\mu V K^{-1}$ and 1910 ± 146 S cm^{-1}, respectively. The substrate-free thermoelectric generator is composed of six n-type and five p-type thermoelectric strips with a length of 2 cm and width of 0.3 cm (Figure S6). The alternating n-type and p-type thermoelectric elements were electrically connected using the SWCNT adhesive. Substrate-free thermoelectric elements were integrated without waste volume. Figure 4b shows the output voltage−output current and output power−output current curves of the thermoelectric generator. The substrate-free, flexible thermoelectric generator exhibits a maximum power of 0.38, 2.4, and 6.1 μW at ΔT values of 8, 20, and 35 K, respectively. A substrate-free, flexible thermoelectric generator with a free-standing Ag_2Se film for effective energy harvesting was successfully demonstrated. The internal resistance of the thermoelectric generator was measured to be 36 Ω, which is higher than the calculated total resistance of the thermoelectric elements, 24 Ω. There should be contact resistance between the thermoelectric elements. The maximum output power, which is inversely proportional to the internal resistance, can increase by reducing the contact resistance. In addition, the device performance can increase further if the p-type elements are replaced with better performance materials. Thus, development of high-performance p-type flexible thermoelectric films is highly demanded. We demonstrated a simple in-plane thermoelectric generator. Vertical-type thermoelectric generators for effective harvesting of energy from vertical ΔT can also be fabricated by using flexible thermoelectric films.[18−21]

CONCLUSIONS

Herein, the fabrication of flexible, free-standing Ag_2Se films, and their thermoelectric performance and flexibility are reported. The electrical conductivity, Seebeck coefficient, and thermal conductivity of the free-standing Ag_2Se films were measured with in-plane direction. The zT of the free-standing Ag_2Se films with a thickness of 25.0 ± 3.9 μm was 0.514 ± 0.060 at room temperature. The free-standing Ag_2Se films exhibited superior flexibility compared to Ag_2Se films constrained on a substrate because a smaller bending strain was applied to the free-standing films. Using free-standing Ag_2Se films, a substrate-free, flexible thermoelectric generator was fabricated. High-density integration of thermoelectric elements and energy harvesting capability were successfully demonstrated.

MATERIALS AND METHODS

Materials. Selenium dioxide (98%), β-cyclodextrin (≥97%), and L-ascorbic acid were purchased from Sigma-Aldrich. Silver nitrate (99.8%), ethanol (94.5%), ethylene glycol (99.5%), and chloroform (99.5%) were purchased from Samchun Chemicals. SWCNTs (Tuball, ≥80%) were purchased from OCSiAl. All chemicals were used as received.

Fabrication of Ag_2Se Microparticles. To prepare solution A, 2 g of selenium dioxide and β-cyclodextrin were dissolved in 400 mL of distilled water. To prepare solution B, 10 g of L-ascorbic acid was dissolved in 400 mL of distilled water. Solution A was then added slowly to solution B using a burette and stirred for 4 h. Next, the dispersion was centrifuged and washed repeatedly with distilled water and ethanol. The obtained solid product was dispersed overnight in 800 mL of ethanol. The dispersion was then centrifuged and washed several times with ethanol. Solid Se nanowires were then obtained by drying overnight in vacuo at 80 °C (Figure S7). The obtained Se nanowires were dispersed in 800 mL of ethylene glycol, and an aqueous $AgNO_3$ solution with an Ag to Se molar ratio of 2 was added. After stirring for 4 h, the dispersion was centrifuged and washed several times with ethanol. Subsequently, solid Ag_2Se microparticles were obtained by drying overnight in vacuo at 80 °C.

Fabrication of Free-Standing Ag_2Se Films. A total of 2.8 g of Ag_2Se microparticles and 16 mL of chloroform were mixed using a

https://doi.org/10.1021/acsami.2c20115
ACS Appl. Mater. Interfaces 2023, 15, 3047−3053

ball milling system (MM400, Retsch) at 20 Hz for 25 min with five zirconia beads with a diameter of 5 mm. The well-dispersed ink was drop-cast onto a polyimide substrate with a size of 15 cm × 10 cm and then dried at room temperature. After hot-pressing the as-prepared film at 230 °C and 5 MPa for 5 min, the Ag_2Se film was peeled off from the polyimide substrate. For fabrication of the Ag_2Se film constrained on a substrate, the same method was used except that a well-dispersed ink composed of 0.175 g of Ag_2Se microparticles and 1 mL of chloroform were drop-cast on a polyvinylidene difluoride (PVDF) membrane filter with a size of 3.75 cm × 2.5 cm.

Fabrication of Substrate-Free Thermoelectric Generator. To obtain the p-type SWCNT film, 1 wt % SWCNT/ethanol paste was prepared using a ball milling system at 30 Hz for 60 min. The paste was then bar-coated on a filter paper with a gap size of 1 mm, dried, and then peeled off. To obtain the conductive adhesive, 1 wt % SWCNT/chloroform paste was prepared using a ball milling system. The p- and n-type thermoelectric elements were electrically connected using the SWCNT adhesive.

Characterization. The Seebeck coefficient was measured at room temperature using a custom-built measurement system. ΔV was measured using a Keithley 2182A nanovoltmeter. ΔT was controlled by two Peltier plates, whose temperatures were controlled using a Keithley 2700 multimeter and a Keithley 2604 B source meter (Figure S8). The Seebeck coefficient was obtained from the slope of the $\Delta V-\Delta T$ curve (Figure S9). The Seebeck coefficient was also measured using Linseis LSR-3 equipment to validate the values measured using a custom-built measurement system. Electrical conductivity, carrier concentration, and mobility were measured using a Hall effect measurement system (HMS-3000, Ecopia). In-plane thermal diffusivity (λ) was measured using an AC thermal diffusivity measurement system (LaserPIT-M2, Advance Rico). The heat capacity (C_p) was measured by conducting differential scanning calorimetry (DSC 204 F1 Phoenix, Netzsch). The thermal conductivity was calculated using the relationship $\kappa = d\lambda C_p$, where d is the density. SEM images were obtained using a Hitachi S4800 operated at 15 kV and an FEI Nova 200 operated at 20 kV. XRD patterns were acquired using a MiniFlex 600 diffractometer (Rigaku) operated at 40 kV and 15 A. The ICP−OES analysis was performed using an iCAP PRO XP DUO instrument (Thermo Fisher Scientific). The XPS analysis was performed using a Nexsa G2 surface analysis system (Thermo Fisher Scientific). TEM images were obtained using a Tecnai G2 F20 instrument operated at 200 kV. The tensile stress−strain curves were obtained using a micromechanical tester (5848, Instron).

■ ASSOCIATED CONTENT

Supporting Information

The Supporting Information is available free of charge at https://pubs.acs.org/doi/10.1021/acsami.2c20115.

XPS spectra of Ag_2Se film; SEM image of the Ag_2Se film constrained on a membrane filter substrate; chemical stability tests of Ag_2Se films; tensile stress−strain curve of the membrane substrate; SEM image of the SWCNT film; device scheme; SEM image and XRD pattern of Se nanowires; photographs of the Seebeck coefficient measurement system; and $\Delta V-\Delta T$ curve of the Ag_2Se film (PDF)

■ AUTHOR INFORMATION

Corresponding Authors

Jungwon Kim − *Institute of Advanced Composite Materials, Korea Institute of Science and Technology (KIST), Wanju 55324, Republic of Korea*; Email: jungwon@kist.re.kr

Kwang-Suk Jang − *Department of Applied Chemistry and Center for Bionano Intelligence Education and Research, Hanyang University, Ansan 15588, Republic of Korea*; orcid.org/0000-0001-5835-9364; Email: kjang@hanyang.ac.kr

Authors

Dongchan Lee − *Department of Applied Chemistry and Center for Bionano Intelligence Education and Research, Hanyang University, Ansan 15588, Republic of Korea*

Woomin Park − *Department of Applied Chemistry and Center for Bionano Intelligence Education and Research, Hanyang University, Ansan 15588, Republic of Korea*

Yeong A Kang − *Institute of Advanced Composite Materials, Korea Institute of Science and Technology (KIST), Wanju 55324, Republic of Korea*

Hyeong Taek Lim − *Institute of Advanced Composite Materials, Korea Institute of Science and Technology (KIST), Wanju 55324, Republic of Korea; Department of Semiconductor Science and Technology/Semiconductor Physics Research Center, Chonbuk National University, Jeonju 54896, Republic of Korea*

Seungbeom Park − *Department of Applied Chemistry and Center for Bionano Intelligence Education and Research, Hanyang University, Ansan 15588, Republic of Korea*

Yeongjun Mun − *Department of Applied Chemistry and Center for Bionano Intelligence Education and Research, Hanyang University, Ansan 15588, Republic of Korea*

Complete contact information is available at: https://pubs.acs.org/10.1021/acsami.2c20115

Author Contributions

[‖]D.-C.L. and W.P. contributed equally to this work.

Notes

The authors declare no competing financial interest.

■ ACKNOWLEDGMENTS

This work was supported by the Basic Research Program through the National Research Foundation of Korea (NRF) funded by the MSIT (2020R1A4A4079870) and the GRRC program of Gyeonggi province (GRRCHanyang2020-B01).

■ REFERENCES

(1) Peng, J.; Snyder, G. J. A Figure of Merit for Flexibility. *Science* **2019**, *366*, 690−691.

(2) Du, Y.; Xu, J.; Paul, B.; Eklund, P. Flexible Thermoelectric Materials and Devices. *Appl. Mater. Today* **2018**, *12*, 366−388.

(3) Wang, Y.; Yang, L.; Shi, X.-L.; Shi, X.; Chen, L.; Dargusch, M. S.; Zou, J.; Chen, Z.-G. Flexible Thermoelectric Materials and Generators: Challenges and Innovations. *Adv. Mater.* **2019**, *31*, 1807916.

(4) Paul, B.; Lu, J.; Eklund, P. Nanostructural Tailoring to Induce Flexibility in Thermoelectric $Ca_3Co_4O_9$ Thin Films. *ACS Appl. Mater. Interfaces* **2017**, *9*, 25308−25316.

(5) Paul, B.; Björk, E. M.; Kumar, A.; Lu, J.; Eklund, P. Nanoporous $Ca_3Co_4O_9$ Thin Films for Transferable Thermoelectrics. *ACS Appl. Energy Mater.* **2018**, *1*, 2261−2268.

(6) Saeidi-Javash, M.; Kuang, W.; Dun, C.; Zhang, Y. 3D Conformal Printing and Photonic Sintering of High-Performance Flexible Thermoelectric Films Using 2D Nanoplates. *Adv. Funct. Mater.* **2019**, *29*, 1901930.

(7) Hollar, C.; Lin, Z.; Kongara, M.; Varghese, T.; Karthik, C.; Schimpf, J.; Eixenberger, J.; Davis, P. H.; Wu, Y.; Duan, X.; Zhang, Y.; Estrada, D. High-Performance Flexible Bismuth Telluride Thin Film from Solution Processed Colloidal Nanoplates. *Adv. Mater. Technol.* **2020**, *5*, 2000600.

(8) Shang, H.; Dun, C.; Deng, Y.; Li, T.; Gao, Z.; Xiao, L.; Gu, H.; Singh, D. J.; Ren, Z.; Ding, F. $Bi_{0.5}Sb_{1.5}Te_3$-Based Films for Flexible Thermoelectric Devices. *J. Mater. Chem. A* **2020**, *8*, 4552−4561.
(9) Ding, Y.; Qiu, Y.; Cai, K.; Yao, Q.; Chen, S.; Chen, L.; He, J. High Performance n-Type Ag_2Se Film on Nylon Membrane for Flexible Thermoelectric Power Generator. *Nat. Commun.* **2019**, *10*, 841.
(10) Jiang, C.; Ding, Y.; Cai, K.; Tong, L.; Lu, Y.; Zhao, W.; Wei, P. Ultrahigh Performance of n-Type Ag_2Se Films for Flexible Thermoelectric Power Generators. *ACS Appl. Mater. Interfaces* **2020**, *12*, 9646−9655.
(11) Gao, J.; Miao, L.; Lai, H.; Zhu, S.; Peng, Y.; Wang, X.; Koumoto, K.; Cai, H. Thermoelectric Flexible Silver Selenide Films: Compositional and Length Optimization. *iScience* **2020**, *23*, 100753.
(12) Mallick, M. M.; Rösch, A. G.; Franke, L.; Gall, A.; Ahmad, S.; Geßwein, H.; Mazilkin, A.; Kübel, C.; Lemmer, U. New Frontier in Printed Thermoelectrics: Formation of β-Ag_2Se through Thermally Stimulated Dissociative Adsorption Leads to High ZT. *J. Mater. Chem. A* **2020**, *8*, 16366−16375.
(13) Xu, S.; Li, M.; Dai, Y.; Hong, M.; Sun, Q.; Lyu, W.; Liu, T.; Wang, Y.; Zou, J.; Chen, Z.-G.; Dargusch, M. Realizing a 10 °C Cooling Effect in a Flexible Thermoelectric Cooler Using a Vortex Generator. *Adv. Mater.* **2022**, *34*, 2204508.
(14) Li, Y.; Lou, Q.; Yang, J.; Cai, K.; Liu, Y.; Lu, Y.; Qiu, Y.; Lu, Y.; Wang, Z.; Wu, M.; He, J.; Shen, S. Exceptionally High Power Factor Ag_2Se/Se/Polypyrrole Composite Films for Flexible Thermoelectric Generators. *Adv. Funct. Mater.* **2022**, *32*, 2106902.
(15) Wei, M.; Shi, X.-L.; Zheng, Z.-H.; Li, F.; Liu, W.-D.; Xiang, L.-P.; Xie, Y.-S.; Chen, Y.-X.; Duan, J.-Y.; Ma, H.-L.; Liang, G.-X.; Zhang, X.-H.; Fan, P.; Chen, Z.-G. Directional Thermal Diffusion Realizing Inorganic Sb_2Te_3/Te Hybrid Thin Films with High Thermoelectric Performance and Flexibility. *Adv. Funct. Mater.* **2022**, *32*, 2207903.
(16) Wu, M.; Cai, K.; Li, X.; Li, Y.; Liu, Y.; Lu, Y.; Wang, Z.; Zhao, W.; Wei, P. Ultraflexible and High-Thermoelectric-Performance Sulfur-Doped Ag_2Se Film on Nylon for Power Generators. *ACS Appl. Mater. Interfaces* **2022**, *14*, 4307−4315.
(17) Li, X.; Lu, K.; Cai, M.; Gao, Y.; Li, Z.; Wang, M.; Wu, P.; Wei, W.; Zhao, Y.; Du, S.; Shen, S. Exceptional Power Factor of Flexible Ag/Ag_2Se Thermoelectric Composite Films. *Chem. Eng. J.* **2022**, *434*, 134739.
(18) Kim, S.; Mo, J.-H.; Jang, K.-S. High-Performance n-Type Carbon Nanotubes Doped by Oxidation of Neighboring Sb_2Te_3 for a Flexible Thermoelectric Generator. *ACS Appl. Mater. Interfaces* **2020**, *12*, 43778−43784.
(19) Kim, S.; Mo, J.-H.; Jang, K.-S. Solution-Processed Carbon Nanotube Buckypapers for Foldable Thermoelectric Generators. *ACS Appl. Mater. Interfaces* **2019**, *11*, 35675−35682.
(20) Hwang, H.; Jang, K.-S. Thermoelectric All-Carbon Heterostructures for a Flexible Thermoelectric Generator. *Sustainable Energy Fuels* **2021**, *5*, 267−273.
(21) Hwang, H.; Mo, J.-H.; Jang, K.-S. Polymer Additive-Combusted Thermoelectric Buckypapers for Three-Dimensional Stacked Paper Thermoelectric Generator. *J. Ind. Eng. Chem.* **2020**, *84*, 260−268.
(22) Romand, M.; Roubin, M.; Deloume, J. P. ESCA Studies of Some Copper and Silver Selenides. *J. Electron Spectrosc. Relat. Phenom.* **1978**, *13*, 229−242.
(23) Mohanty, B. C.; Malar, P.; Osipowicz, T.; Murty, B. S.; Varma, S.; Kasiviswanathan, S. Characterization of Silver Selenide Thin Films Grown on Cr-Covered Si Substrates. *Surf. Interface Anal.* **2009**, *41*, 170−178.
(24) Chen, R.; Xu, D.; Guo, G.; Tang, Y. Electrodeposition of Silver Selenide Thin Films from Aqueous Solutions. *J. Mater. Chem.* **2002**, *12*, 1437−1441.
(25) Shenasa, M.; Sainkar, S.; Lichtman, D. XPS Study of Some Selected Selenium Compounds. *J. Electron Spectrosc. Relat. Phenom.* **1986**, *40*, 329−337.
(26) Conn, J. B.; Taylor, R. C. Thermoelectric and Crystallographic Properties of Ag_2Se. *J. Electrochem. Soc.* **1960**, *107*, 977−982.
(27) Ferhat, M.; Nagao, J. Thermoelectric and Transport Properties of β-Ag_2Se Compounds. *J. Appl. Phys.* **2000**, *88*, 813−816.
(28) Duan, H. Z.; Li, Y. L.; Zhao, K. P.; Qiu, P. F.; Shi, X.; Chen, L. D. Ultra-Fast Synthesis for Ag_2Se and CuAgSe Thermoelectric Materials. *JOM* **2016**, *68*, 2659−2665.
(29) Jood, P.; Chetty, R.; Ohta, M. Structural Stability Enables High Thermoelectric Performance in Room Temperature Ag_2Se. *J. Mater. Chem. A* **2020**, *8*, 13024−13037.
(30) Li, D.; Zhang, J. H.; Li, J. M.; Zhang, J.; Qin, X. Y. High Thermoelectric Performance for an Ag_2Se-Based Material Prepared by a Wet Chemical Method. *Mater. Chem. Front.* **2020**, *4*, 875−880.
(31) Gleskova, H.; Wagner, S.; Suo, Z. a-Si TFTs Made on Polyimide Foil by PE-CVD at 150 °C. *MRS Online Proc. Libr.* **2011**, *508*, 73−78.
(32) Kim, T.-W.; Lee, J.-S.; Kim, Y.-C.; Joo, Y.-C.; Kim, B.-J. Bending Strain and Bending Fatigue Lifetime of Flexible Metal Electrodes on Polymer Substrates. *Materials* **2019**, *12*, 2490.

https://doi.org/10.1021/acsami.2c20115
ACS Appl. Mater. Interfaces 2023, 15, 3047−3053